Processing and Application of Ceramics 11 [4] (2017) 282–289
https://doi.org/10.2298/PAC1704282A

$Ce_{1-x}Fe_xO_2$ nanocatalysts for priority organic pollutants removal through catalytic wet air oxidation

Anushree*, Chhaya Sharma, Satish Kumar

Indian Institute of Technology Roorkee, 247667 Roorkee, India

Received 2 June 2017; Received in revised form 14 September 2017; Accepted 17 November 2017

Abstract

A series of $Ce_{1-x}Fe_xO_2$ nanocatalysts, prepared by co-precipitation method, were applied for the catalytic oxidation of priority organic pollutants present in paper industry wastewater. To investigate the synergic effect of various Fe contents, detailed characterizations of $Ce_{1-x}Fe_xO_2$ were done by Raman, XPS, XRD, TEM and EDX techniques. The addition of Fe to CeO_2 lattice increased the amount of oxygen vacancies, which have an efficient role in the oxidation of organic pollutants under oxygen-rich conditions. $Ce_{0.4}Fe_{0.6}O_2$ catalyst showed the highest removal of TOC (72%), AOX (68%), chlorophenols (62%) and chloroguaicols (86%). The superior catalytic activity of $Ce_{0.4}Fe_{0.6}O_2$ is ascribed to its higher oxygen vacancy concentration. The presence of two oxidation states of Ce (4+,3+) and Fe (3+,2+) confirmed the role of redox couples in oxidation of organic pollutants.

Keywords: *$Ce_{1-x}Fe_xO_2$, nanocatalyst, oxygen vacancy, wet air oxidation, chlorophenolics*

I. Introduction

Today, the water pollution has become a global menace. The discharge of untreated industrial wastewaters is the main cause behind water pollution [1]. The increasing fresh water demand and stringent regulations have forced the industry to adopt the treatment techniques prior to discharge of wastewater to the environment. Biological methods have been widely explored, but the presence of non-biodegradable and toxic compounds in industrial wastewaters limits their application [2]. Catalytic wet air oxidation (CWAO) has a lot of potential towards the oxidation of organic compounds present in industrial wastewaters. High operating temperature and pressure limit the application of CWAO, confronted with the special equipment [3,4]. The development of catalyst with high activity in CWAO under mild reaction conditions is still a challenging task [5]. Metal oxides are important class of catalysts and they are widely reported to serve as a substitute to the noble metals for various catalytic reactions. Recently, CeO_2 has attracted a considerable interest as an environmental catalyst. The activity of CeO_2 is due to its oxygen vacancy defects and high oxygen storage capacity associated with the facile transformation between Ce^{4+} and Ce^{3+} [6]. However, poor thermal stability of the pure CeO_2 is disadvantageous for catalysis. The mixed metal oxides (MMOs) of CeO_2 with various transition metals have demonstrated the better oxygen storage capacity and catalytic properties than the pure CeO_2 [7,8]. In general, the activity of a catalyst is associated with various structural factors, like chemical composition, specific surface area and surface oxygen vacancies [9]. The nanomaterials are reported to exhibit the high activity and stability in catalytic reactions, mainly due to their high specific surface area and better dispersion of active components. Therefore, nanocrystalline ceria-transition metals (MMOs) can be thought as an efficient heterogeneous catalyst for CWAO. Here Fe was selected for the formation of MMOs with CeO_2, as Fe-based materials are particularly appealing in the field of catalysis [10–12].

In this study, the $Ce_{1-x}Fe_xO_2$ nanocatalysts were investigated for catalytic wet air oxidation of paper industry wastewater through CWAO. The relationship between structural properties and oxidation behaviours of $Ce_{1-x}Fe_xO_2$ mixed oxides was established by different characterization techniques.

* Corresponding author: tel: +91 7290807066,
e-mail: *anushreejatrana@gmail.com*

II. Material and methods

2.1. Wastewater sample

The wastewater sample was collected from primary clarifier outlet of a paper industry. The paper industry wastewater is highly polluted and characterized by high total organic carbon (TOC). The chlorinated compounds generated during bleaching are in particular the most harmful toxicants. Various chlorinated organic compounds identified in paper industry wastewater include chlorinated hydrocarbons, chloroform, furans, dioxins, chlorophenols etc. [13,14]. These chlorinated compounds are collectively estimated as adsorbable organic halides (AOX). Out of these, chlorophenolic compounds and their derivatives are major environmental concern, due to their persistence and adverse effects including carcinogenicity, dermal adsorption paralysis, injurious effects on reproductive and haematological organs of humans and the ecobiota [15,16]. Some of these compounds have been classified as priority pollutants by EPA, US [17]. The chlorophenols (CP) and chloroguaiacols (CG) are quantitatively significant chlorophenolic compounds in paper industry wastewater [18].

2.2. Catalyst synthesis and characterization

The $Ce_{1-x}Fe_xO_2$ nanocatalysts with different Fe content (x = 0.2, 0.4, 0.6, 0.8) were prepared by co-precipitation method [19]. The pure CeO_2 and Fe_2O_3 catalysts were also synthesized. The catalysts were characterized by XRD, TEM, EDX, Raman and XPS techniques. The XRD pattern were recorded on Bruker AXS D8 X-ray diffractometer equipped with CuKα radiation (λ = 0.154 nm). TEM analysis was carried out on Tecnai G^2 STWIN microscope operating at an accelerating voltage of 200 kV. The EDX analysis was done by Oxford Instruments, 51 XMX 1005. Raman analysis was performed on Invia Renishaw spectrometer at 514 nm excitation line of Ar ion laser. The XPS spectra were obtained by PHI 5000 Versa Probe instrument.

2.3. Analytical methods

The TOC value of the wastewater sample was measured by Shimadzu TOC-L CPH analyser, where the difference between total carbon (TC) and total inorganic carbon (IC) gave the TOC value. AOX value was analysed by a Dextar AOX analyser based on combustion ion chromatography. The chlorophenolic compounds (CHPs) were quantified by GC-MS (Trace GC Ultra-DSQ, Thermo Electron Corporation) equipped with a TR-5 capillary column. CHPs were first extracted from the wastewater by liquid-liquid extraction method and then derivatized by acetic anhydride. The quantitative analysis of CHPs was carried out with the help of calibration curve of standard compounds.

III. Results and discussion

3.1. Structural characterization

Figure 1 presents the XRD pattern of CeO_2, Fe_2O_3 and $Ce_{1-x}Fe_xO_2$ nanocatalysts. The diffraction pattern for CeO_2 matches well with the characteristic cubic phase (JCPDS 81-0792). Fe_2O_3 presented the characteristic reflections of tetragonal hematite structure (JCPDS 86-0550). For $Ce_{1-x}Fe_xO_2$ nanocatalysts, the peaks corresponding to Fe_2O_3 phase appeared in the sample with 80 at.% Fe, indicating the solid solubility of Fe_2O_3 into CeO_2 up to 60 at.% [19]. For $Ce_{1-x}Fe_xO_2$ nanocatalysts, the characteristic ceria peaks were shifted towards higher values indicating the lattice deformation due to the presence of oxygen vacancies.

Raman spectroscopy was carried out to characterize the oxygen vacancies within catalysts. Raman spectra of $Ce_{1-x}Fe_xO_2$ nanocatalysts are presented in Fig. 2. CeO_2 exhibited a prominent F_{2g} peak at 460 cm^{-1}, corresponding to the symmetric breathing mode of oxygen atoms around cerium ions (Ce^{4+}) [20]. For $Ce_{1-x}Fe_xO_2$ nanocatalysts, a less-prominent broad band was observed in the range from 530 to 740 cm^{-1}. This

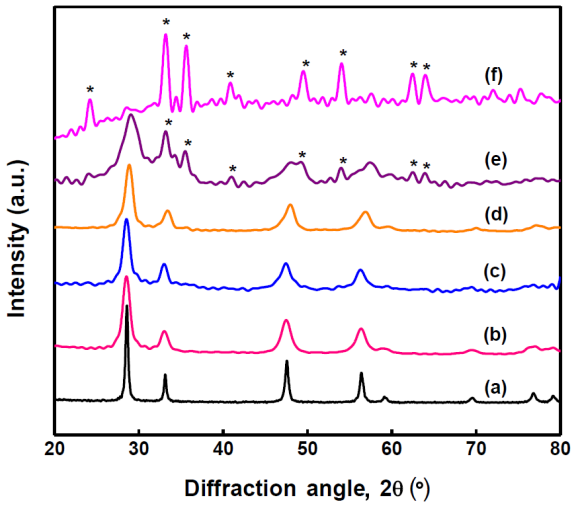

Figure 1. XRD pattern of catalysts: a) CeO_2, b) $Ce_{0.8}Fe_{0.2}O_2$, c) $Ce_{0.6}Fe_{0.4}O_2$, d) $Ce_{0.4}Fe_{0.6}O_2$, e) $Ce_{0.2}Fe_{0.8}O_2$ and f) Fe_2O_3

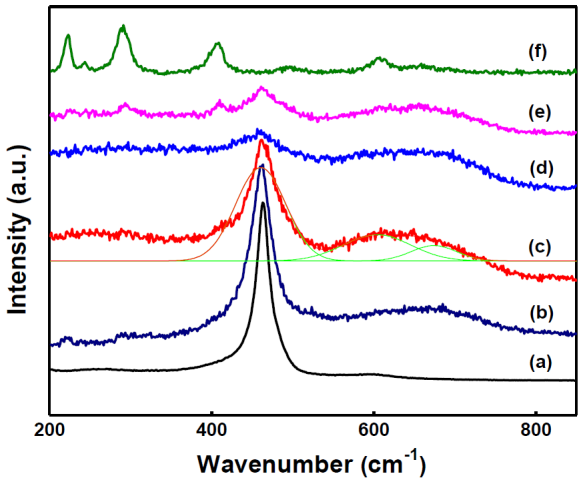

Figure 2. Raman spectra of catalysts: a) CeO_2, b) $Ce_{0.8}Fe_{0.2}O_2$, c) $Ce_{0.6}Fe_{0.4}O_2$, d) $Ce_{0.4}Fe_{0.6}O_2$, e) $Ce_{0.2}Fe_{0.8}O_2$ and f) Fe_2O_3

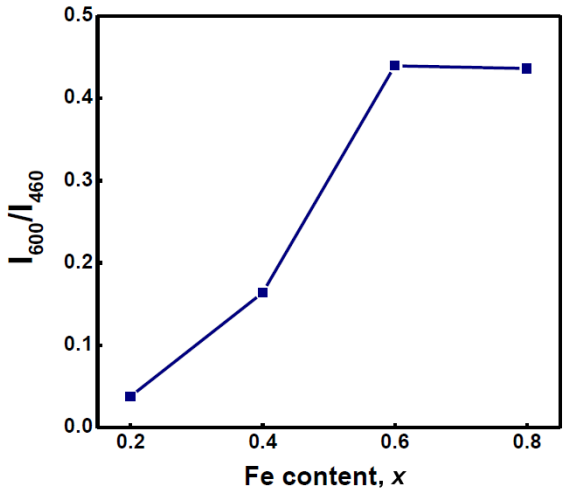

Figure 3. Variation of I_{600}/I_{460} with Fe content

broad band was deconvoluted into two bands centred at 600 cm^{-1} and 675 cm^{-1}, respectively. The first band at 600 cm^{-1} was related to the intrinsic oxygen vacancies which are formed due to the presence of Ce^{3+} [21]. In particular, this band was attributed to the Raman inactive LO mode caused by relaxation of symmetry selection rules. The second weak band at 675 cm^{-1} indicated the presence of small amount of Fe_3O_4 in the surface layer of nanocatalysts [22]. The shifting of Raman peaks towards lower wavenumber indicates the increase in oxygen vacancies, which is related to the structural defects derived from the incorporation of Fe into CeO_2 lattice. The concentration of oxygen vacancies for all samples was compared by calculating the intensity ratio I_{600}/I_{460} of bands at 600 and 460 cm^{-1}. Figure 3 shows the variation of I_{600}/I_{460} as a function of Fe concentration. The intensity ratio I_{600}/I_{460} increased with increasing Fe content and reached a maximum for $Ce_{0.4}Fe_{0.6}O_2$ mixed oxide. The value of I_{600}/I_{460} was high [23,24] and indicates the appreciably high concentration of oxygen vacancies. Fe_2O_3 exhibited the Raman peaks at 225, 245, 292, 408 and 497 cm^{-1}, corresponding to α-Fe_2O_3 [25].

The oxidation state of metal ions in $Ce_{0.4}Fe_{0.6}O_2$ nanocatalysts was confirmed by XPS analysis. Ce 3d spectra (Fig. 4a) exhibited the three main 3 $d_{5/2}$ features at the binding energies of 881.8, 887.6 and 897.4 eV corresponding to v, v", v"' components, respectively. The 3 $d_{3/2}$ feature corresponding to u, u" and u"' components were observed at 899.9, 906.1 and 915.7 eV. The v, v", v"', u, u" and u"' peaks with v and u splitting of 18.4 eV are the characteristic of Ce^{4+} oxidation state (CeO_2). Additional peaks corresponding to v' (884 eV), u' (902 eV), v° (880.8 eV) and u° (899 eV) components indicated the presence of Ce^{3+}. The XPS results suggest that there is a certain amount of Ce^{3+} [26]. The atomic fraction of Ce^{3+} calculated from the integrated peak areas was found to be 28 at.%. This percentage indicates the presence of the significant number of oxygen vacancies [27,28]. Figure 4b presents the Fe 2p core level binding energy spectra for $Ce_{0.4}Fe_{0.6}O_2$ nanocatalyst. After refined fitting, the spectrum was deconvoluted into four peaks with strong binding energies centred at around 709.4 and 723 eV assigned to Fe^{2+}. The peaks centred at about 711.5 and 725 eV can be ascribed to the presence of Fe^{3+}. The spectra also exhibited well-defined shake-up satellite peaks at 716.8 eV and 731.7 eV [29,30]. These results suggest the coexistence of Fe^{2+}/Fe^{3+} ion couple in $Ce_{1-x}Fe_xO_2$ nanocatalysts. O 1s spectra (Fig. 4c) exhibited three components, the relative percentage of each component is provided in parenthesis. The peak centred at 528.5 eV was related to the lattice oxygen (69.5%). The peak at 531.4 eV indicated the presence of adsorbed surface oxygen in the form of OH^- ions (9.4%). The additional peak at 530.2 eV was related to the supercharged oxygen (O_2^-) near the oxygen vacant sites at the surface (21%) [31]. These results suggest that the $Ce_{1-x}Fe_xO_2$ nanocatalysts have better oxygen storage capacity, which would be advantageous for their higher catalytic oxidation activity.

Thus, Raman and XPS results revealed that the oxygen vacancies were generated by the incorporation of Fe ion into the ceria lattice to compensate the valence mismatch between the Fe^{2+}/Fe^{3+} and Ce^{3+}/Ce^{4+} ions. These results also provide evidence for the existence of redox equilibrium of $Fe^{3+} + Ce^{3+} \longleftrightarrow Fe^{2+} + Ce^{4+}$, which is the source of a synergistic interaction between iron and ceria species in the $Ce_{1-x}Fe_xO_2$ nanocatalysts.

The morphology and microstructure of nanocatalysts

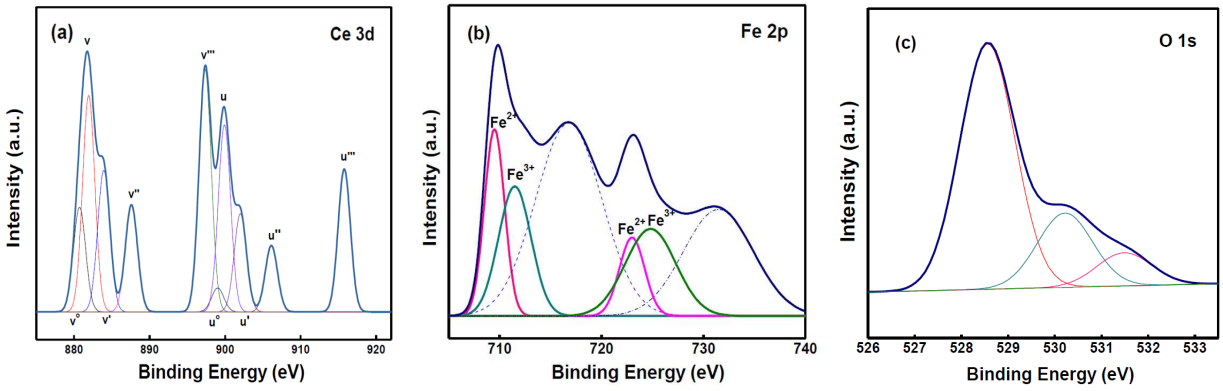

Figure 4. Fitted XPS spectra of $Ce_{0.4}Fe_{0.6}O_2$ mixed oxide: a) Ce 3d, b) Fe 2p and c) O 1s

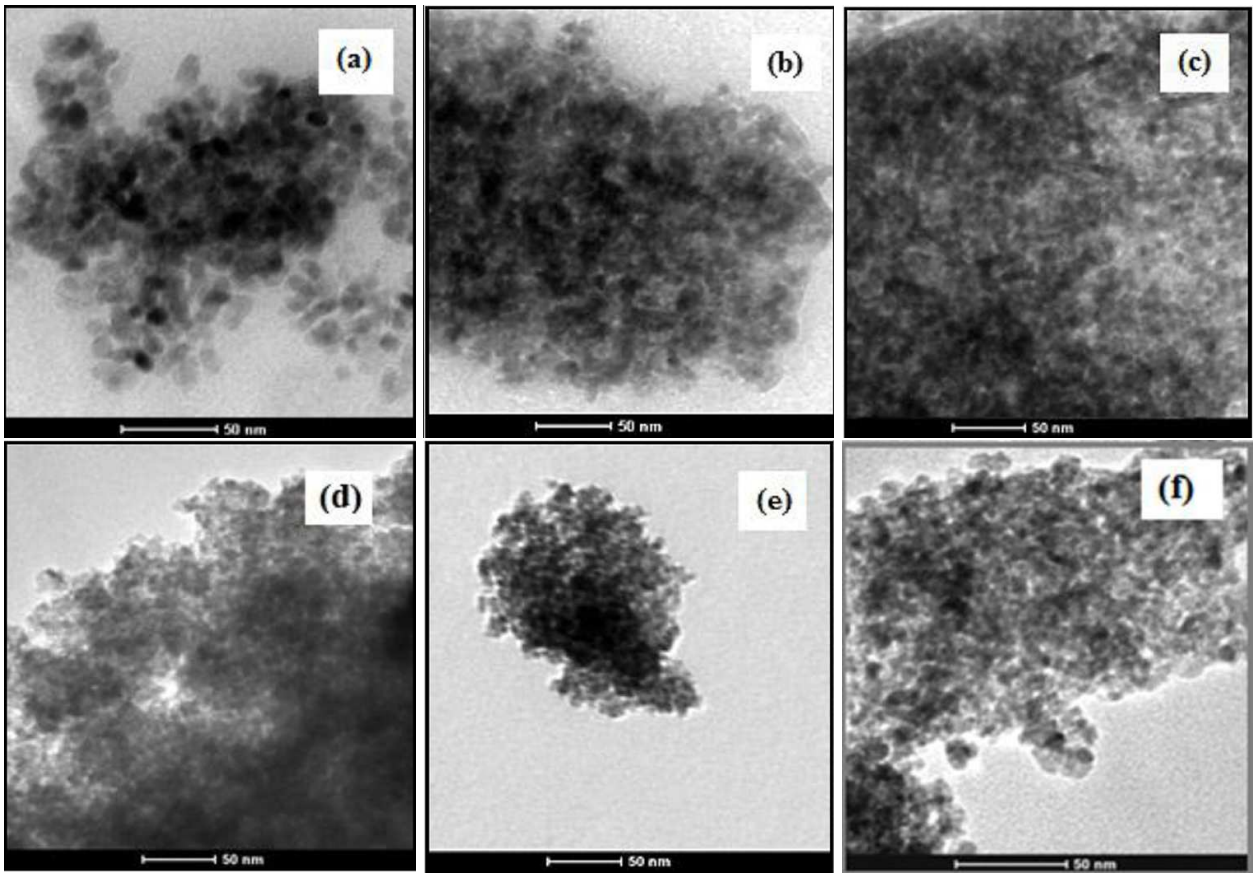

Figure 5. TEM images of catalysts: a) CeO_2, b) $Ce_{0.8}Fe_{0.2}O_2$, c) $Ce_{0.6}Fe_{0.4}O_2$, d) $Ce_{0.4}Fe_{0.6}O_2$, e) $Ce_{0.2}Fe_{0.8}O_2$ and f) Fe_2O_3

were studied by TEM analysis. TEM micrographs of samples are shown in Fig. 5, and the particle sizes measured from micrographs are given in Table 1. The micrographs clearly illustrate that all the samples are aggregated nanoparticles with non-uniform pores. The average particle size of CeO_2 was 11 nm, where most of the particles were spherical and some were elongated in shape. For $Ce_{1-x}Fe_xO_2$ MMOs, the particles are nearly uniform spheres with diameters in the range of 8 to 5 nm. The decrease in particle size with addition of Fe can be related to the inhibition of growth of nanocrystals in presence of Fe ions [32]. Fe_2O_3 particles are also near uniform spheres but slightly larger than those of $Ce_{1-x}Fe_xO_2$ MMOs.

The elemental mapping results illustrate that the samples are MMOs. The quantitative EDX analysis confirmed that the actual Ce/Fe mole ratio in the catalysts was close to the expected values (Table 1).

3.2. Catalyst activity

The paper industry wastewater presented high organic load in terms of TOC (172 mg/l), AOX (16.2 mg/l), CPs (275 μg/l) and CGUs (193 μg/l) [33]. To investigate the catalytic properties of $Ce_{1-x}Fe_xO_2$ nanocatalysts, their catalytic wet air oxidation activity (CWAO) was explored. The CWAO of the wastewater sample was carried out under oxygen-rich conditions in a glass reactor at atmospheric pressure, catalyst dose 1 g/l, pH ~4, temperature 90 °C and reaction time 2 h [19]. Aliquots were taken out after treatment and the catalyst was separated by centrifugation. For comparison, the CWAO activity of the pure CeO_2 and Fe_2O_3 was also investigated under the same conditions.

TOC and AOX removal

Figure 6 presents the abatement of TOC and AOX by CWAO using CeO_2, $Ce_{0.8}Fe_{0.2}O_2$, $Ce_{0.6}Fe_{0.4}O_2$,

Table 1. Crystallite size (from XRD), particle size (from TEM) and elemental analysis (EDS) of catalysts

Sample	Crystallite size [nm]	Particle size [nm]	Ce/Fe molar ratio	
			Expected	Obtained
CeO_2	24	19 ± 2	–	–
$Ce_{0.8}Fe_{0.2}O_2$	8.7	8.9 ± 0.3	4	4.1
$Ce_{0.6}Fe_{0.4}O_2$	8.9	8.2 ± 0.2	1.5	1.6
$Ce_{0.4}Fe_{0.6}O_2$	8.2	7.8 ± 0.5	0.66	0.63
$Ce_{0.2}Fe_{0.8}O_2$	5.3	5.1 ± 0.2	0.25	0.25
Fe_2O_3	11	9.8 ± 0.4	–	–

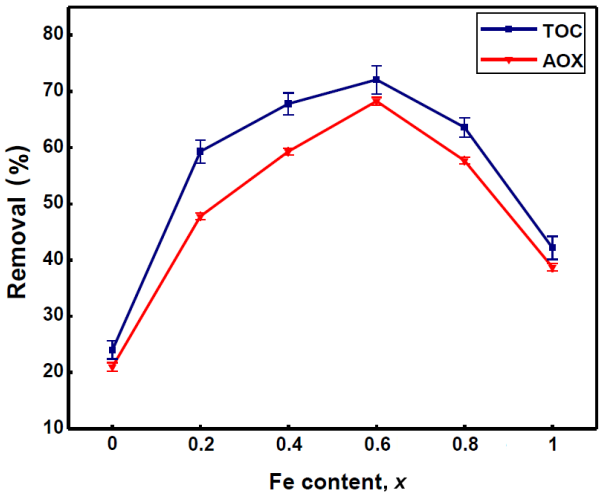

Figure 6. Effect of Fe content on TOC and AOX removal

$Ce_{0.4}Fe_{0.6}O_2$, $Ce_{0.2}Fe_{0.8}O_2$ and Fe_2O_3. CeO_2 was found to be the least active catalyst with 24% TOC and 21% AOX abatement. Fe_2O_3 catalyst also exhibited the low abatement profile with 42% TOC and 38% AOX abatement. All the mixed catalysts exhibited higher removal efficiency, which increased with increasing Fe content and reached the maximum with Ce/Fe mole ratio of 40/60 (72% TOC and 68% AOX). The results show that the incorporation of Fe in CeO_2 can promote the catalytic activity, which could be interpreted in terms of synergistic interaction between iron and ceria species in $Ce_{1-x}Fe_xO_2$ nanocatalysts.

The highest efficiency of $Ce_{0.4}Fe_{0.6}O_2$ can be ascribed to the high oxygen vacancy concentration, as indicated by Raman analysis. On the basis of Raman and XPS results it can be concluded that Ce^{4+} and Fe^{3+} are easily reducible to Ce^{3+} and Fe^{2+}, respectively. These Ce^{3+} and Fe^{2+} ions are the active sites, where the reactant molecule is oxidized by the interface lattice oxygen, generating the oxygen vacancy. The oxygen vacancy is filled up by the gaseous O_2, forming adsorbed active oxygen species which can react with another reactant molecule. Thus, the oxygen vacancies lead to the high oxygen mobility which is the main factors influencing the activity of catalytic oxidation.

Chlorophenols (CPs) removal

GC-MS analysis of chlorophenolics revealed the presence of total 13 chlorophenols (CPs) in the paper industry wastewater. The contribution from monochlorophenols (MCPs), di-chlorophenols (DCPs), trichlorophenols (TCPs) and penta-chlorophenols (PCPs) was 7.7%, 41%, 51% and 0.14%, respectively (Fig. 7a). Total amount of chlorophenols was 275 µg/l with major share of 2,4,5-TCP (132.9 µg/l), 2,5-DCP (62.4 µg/l), 2,4-DCP (26.5 µg/l) and 2,6-DCP (22.9 µg/l), while the rest of CPs were present in relatively lower quantities. Based on TOC and AOX removal efficiency, the $Ce_{0.4}Fe_{0.6}O_2$ mixed oxide was selected for the CWAO of chlorophenolics. After CWAO, a noticeable removal

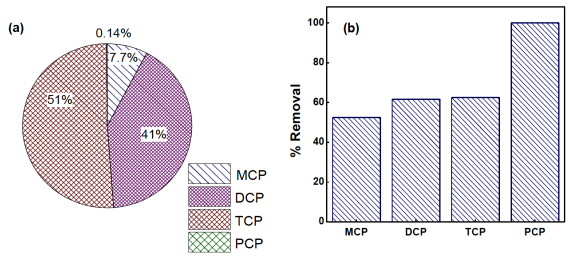

Figure 7. Chlorophenols: a) initial concentration before CWAO and b) concentration after CWAO

Table 2. Concentration of CHPs in paper industry wastewater before and after CWAO

Compound	Before CWAO [µg/l]	After CWAO [µg/l]	[%] removal
3-CP	14.9 ± 10.98	7.5 ± 1.52	50
4-CP	6.2 ± 4.55	2.5 ± 0.31	59
2,3-DCP	0.8 ± 0.01	0.1 ± 0.10	87
2,4-DCP	26.5 ± 0.47	10.8 ± 0.78	59
2,5-DCP	62.4 ± 0.78	26.2 ± 1.15	58
2,6-DCP	22.9 ± 4.45	6.3 ± 1.09	72
3,4- DCP	0.6 ± 0.08	0.02 ± 0.03	96
2,3,4- TCP	3.3 ± 0.10	0.4 ± 0.13	87
2,3,5- TCP	2.5 ± 0.03	1.8 ± 0.10	26
2,3,6- TCP	1.2 ± 0.01	0.9 ± 0.16	25
2,4,5- TCP	132.9 ± 19.7	49.5 ± 1.33	63
2,4,6- TCP	0.4 ± 0.03	0.05 ± 0.02	86
PCP	0.4 ± 0.02	Not Detected	100
Total	275	106	62

of CPs (62%) was achieved. The removal of individual CPs is given in Table 2. Results indicate that the removal of most of CPs was from 50% to 100%. PCP was completely removed or its concentration fallen below the detection limit of instrument. 3,4-DCP was removed up to 96%, followed by 2,3,4-TCP (87%), 2,3-DCP (87%), 2,4,6-TCP (86%), 2,6-DCP (72%), 2,4,5-TCP (63%), 2,4-DCP (59%), 4-CP (59%), 2,5-DCP (58%) and 3-CP (50%). The rest of the compounds was removed up to 24–26% only. Based on Cl substitution, the removal of PCPs, TCPs, DCPs and MCPs was 100%, 62%, 62% and 53%, respectively (Fig. 7b).

Chloroguaicols (CGUs) removal

A total amount of 193 µg/l of chloroguaicols (CGUs) was detected in paper industry wastewater, with major share from 4,5-DCGU (103 µg/l) and 4-CGU (84 µg/l), while the rest of CGUs was present in relatively very low quantity. The di-chloroguaicols (DCGUs), monochloroguaicols (MCGUs), tri-chloroguaicols (TCGUs) and tetra-chloroguaicols (TeCGUs) comprised 55%, 43%, 0.97% and 0.94% of the total amount of CGUs (Fig. 8a).

After CWAO 86% removal of CGUs was observed. The removal of each individual CGU is presented in Table 3. The results indicate that the removal of most of CGUs was from 81% to 100%. Maximum removal efficiency was achieved for 4,5-DCGU (89%), followed

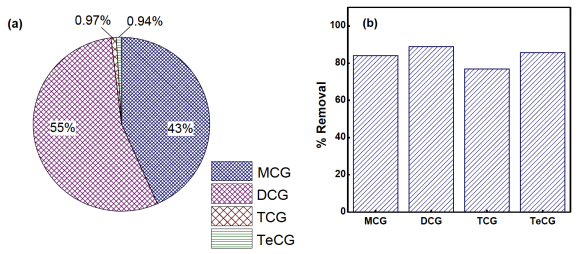

Figure 8. Chloroguaicols: a) initial concentration before CWAO and b) concentration after CWAO

Table 3. Concentration of chloroguaicols in paper industry wastewater before and after CWAO

Compound	Before CWAO [µg/l]	After CWAO [µg/l]	[%] removal
4-CG	83.6 ± 19.5	13.3 ± 1.2	84
4,5-DCG	103 ± 1.9	11.6 ± 1.9	89
4,6-DCG	2.6 ± 0.5	1.2 ± 0.04	56
3,4,5-TCG	0.6 ± 0.1	0.4 ± 0.4	33
3,4,6-TCG	0.5 ± 0.2	ND	100
4,5,6-TCG	0.7 ± 0.1	0.1 ± 0.02	81
Tet-CG	1.8 ± 0.2	0.3 ± 0.05	86
Total	193	27	86

by Tet-CGU (86%), 4-CGU (84%), 4,5,6-TCGU (81%) and 4,6-DCGU (56%). Minimum removal of 33% was obtained for 3,4,5-TCGU. Based on Cl atom substitution, the degradation of TeCGUs, TCGUs, DCGUs and MCGUs was 85%, 77%, 89% and 84%, respectively (Fig. 8b).

Various CWAO studies have been reported in presence of ceria based catalysts. Ru/$Ce_{1-x}Zr_xO_2$ catalyst exhibited up to 43% TOC abatement from surface plating industry wastewater at 150 °C and 0.6 MPa [34]. Ag/$Ce_{0.85}Zr_{0.15}O_2$ catalyst achieved 76% removal of bisphenol A at 160 °C and 2 MPa [35]. CeO_2-TiO_2 catalyst showed 100% COD and 77% TOC removal of phenol at 150 °C and 3 MPa [36]. In this line, our result indicates the suitability of $Ce_{1-x}Fe_xO_2$ nanocatalysts for removal of TOC, AOX, chlorophenols and chloroguaicols at mild operating conditions.

3.3. Kinetic studies

The time dependent TOC removal was studied in order to understand the rate of reaction during oxidation. The experimental data obtained with time-dependent TOC removal in presence of $Ce_{0.4}Fe_{0.6}O_2$ catalyst was modelled on the assumption of first-order kinetics, as follows [37]:

$$-\frac{\mathrm{d}\,[\mathrm{TOC}]}{\mathrm{d}\,t} = k_1 \cdot [\mathrm{TOC}] \qquad (1)$$

By integrating Eq. (1):

$$-\int_{[\mathrm{TOC}]_0}^{[\mathrm{TOC}]} \frac{\mathrm{d}\,[\mathrm{TOC}]}{[\mathrm{TOC}]} = k_1 \cdot \int_0^t \mathrm{d}\,t \qquad (2)$$

the following relation can be obtained:

$$\ln \frac{[\mathrm{TOC}]_0}{[\mathrm{TOC}]} = k_1 \cdot t \qquad (3)$$

The experimental data fitted well for the first order kinetics, as straight line with R^2 value of 0.96 was obtained in the plot constructed between $\ln([\mathrm{TOC}]_0/[\mathrm{TOC}])$ and time (t) (Fig. 9). Thus the CWAO of wastewater in presence of $Ce_{1-x}Fe_xO_2$ nanocatalysts was found to follow the first order kinetics.

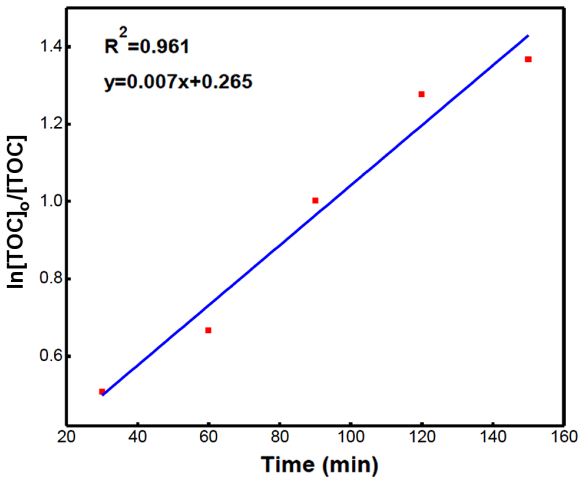

Figure 9. Plot of $\ln([\mathrm{TOC}]_0/[\mathrm{TOC}])$ as a function of reaction time

IV. Conclusions

$Ce_{1-x}Fe_xO_2$ nanocatalysts were synthesized by co-precipitation method. The characteristics of nanocatalysts with different Fe contents were studied by various techniques. The activity of nanocatalysts was explored for the catalytic wet air oxidation of industrial wastewater. The $Ce_{0.4}Fe_{0.6}O_2$ nanocatalyst presented the appreciable removal of TOC, AOX, chlorophenols and chloroguaicols. The characterization results revealed that the presence of Ce^{3+} and Fe^{2+} and richer surface oxygen vacancies are responsible for the better performance of $Ce_{1-x}Fe_xO_2$ nanocatalysts. The results provide an efficient catalyst for removal of priority organic pollutants from the complex industrial wastewater through the catalytic wet air oxidation.

Acknowledgement: The research grant for this study provided by Ministry of Human Resource and Development, Government of India is gratefully acknowledged.

References

1. D. Seckler, R. Barker, U. Amarasinghe, "Water scarcity in the twenty-first century", *Int. J. Water Resour. Develop.*, **15** [1-2] (1999) 29–42.
2. M. Lapertot, C. Pulgarín, P. Fernández-Ibáñez, M.I. Maldonado, L. Pérez-Estrada, I. Oller, W. Gernjak, S. Malato,

"Enhancing biodegradability of priority substances (pesticides) by solar photo-Fenton", *Water Res.*, **40** [5] (2006) 1086–1094.
3. H.T. Gomes, J.L. Figueiredo, J.L. Faria, "Catalytic wet air oxidation of olive mill wastewater", *Catal. Today*, **124** [3] (2007) 254–259.
4. G. Jing, M. Luan, T. Chen, "Progress of catalytic wet air oxidation technology", *Arabian J. Chem.*, **9** (2012) S1208–S1213.
5. J. Levec, A. Pintar, "Catalytic wet-air oxidation processes: a review", *Catal. Today*, **124** [3] (2007) 172–184.
6. T. Montini, M. Melchionna, M. Monai, P. Fornasiero, "Fundamentals and catalytic applications of CeO_2-based materials", *Chem. Rev.*, **116** [10] (2016) 5987–6041.
7. A. Uzunoglu, H. Zhang, S. Andreescu, L.A. Stanciu, "CeO_2-MO_x (M: Zr, Ti, Cu) mixed metal oxides with enhanced oxygen storage capacity", *J. Mater. Sci.*, **50** [10] (2015) 3750–3762.
8. Anushree, S. Kumar, C. Sharma, "Synthesis, characterization and application of CuO-CeO_2 nanocatalysts in wet air oxidation of industrial wastewater", *J. Environ. Chem. Eng.*, **5** [4] (2017) 3914–3921.
9. L.F. Liotta, H. Wu, G. Pantaleo, A.M. Venezia, "Co_3O_4 nanocrystals and Co_3O_4-MO_x binary oxides for CO, CH_4 and VOC oxidation at low temperatures: A review", *Catal. Sci. Technol.*, **3** [12] (2013) 3085–3102.
10. S.W. Cao, Y.J. Zhu, "Hierarchically nanostructured α-Fe_2O_3 hollow spheres: Preparation, growth mechanism, photocatalytic property, and application in water treatment", *J. Phys. Chem. C*, **112** [16] (2008) 6253–6257.
11. Z.M. Cui, Z. Chen, C.Y. Cao, L. Jiang, W.G. Song, "A yolk-shell structured Fe_2O_3@mesoporous SiO_2 nanoreactor for enhanced activity as a Fenton catalyst in total oxidation of dyes", *Chem. Commun.*, **49** [23] (2013) 2332–2334.
12. F. Martínez, J.A. Melero, J.Á. Botas, M.I. Pariente, R. Molina, "Treatment of phenolic effluents by catalytic wet hydrogen peroxide oxidation over Fe_2O_3/SBA-15 extruded catalyst in a fixed-bed reactor", *Ind. Eng. Chem. Res.*, **46** [13] (2007) 4396–4405.
13. D.V. Savant, R. Abdul-Rahman, D.R. Ranade, "Anaerobic degradation of adsorbable organic halides (AOX) from pulp and paper industry wastewater", *Bioresource Technol.*, **97** [9] (2006) 1092–1104.
14. D. Pokhrel, T. Viraraghavan, "Treatment of pulp and paper mill wastewater - A review", *Sci. Total Environ.*, **333** [1] (2004) 37–58.
15. K. Johnsen, J. Tana, K.J. Lehtinen, T. Stuthridge, K. Mattsson, J. Hemming, G.E. Carlberg, "Experimental field exposure of brown trout to river water receiving effluent from an integrated newsprint mill", *Ecotoxicology Environ. Safety*, **40** [3] (1998) 184–193.
16. T.G. Kovacs, P.H. Martel, R.H. Voss, "Assessing the biological status of fish in a river receiving pulp and paper mill effluents", *Environ. Pollution*, **118** [1] (2002) 123–140.
17. V.P. Kozak, G.V. Simsiman, G. Chesters, D. Stensby, J. Harkin, *Reviews of the Environmental Effects of Pollutants: XI. Chlorophenols*, U.S. Environmental Protection Agency, Washington, D.C., EPA/600/1-79/012 (NTIS ORNL), 1979.
18. M.K. Ghosh, U.K. Ghosh, S. Kumar, "Minimization of phenols and phenolic compounds in pulp and paper industries: Biological approaches", *J. Chem. Chem. Eng.*, **5** [7] (2011) 595–607.
19. Anushree, S. Kumar, C. Sharma, "Synthesis, characterization and catalytic wet air oxidation property of mesoporous $Ce_{1-x}Fe_xO_2$ mixed oxides", *Mater. Chem. Phys.*, **155** (2015) 223–231.
20. H. Tan, J. Wang, S. Yuand, K. Zhou, "Support morphology-dependent catalytic activity of Pd/CeO_2 for formaldehyde oxidation", *Environ. Sci. Technol.*, **49** [14] (2015) 8675–8682.
21. Z. Wu, M. Li, J. Howe, H.M. Meyer III, S.H. Overbury, "Probing defect sites on CeO_2 nanocrystals with well-defined surface planes by Raman spectroscopy and O_2 adsorption", *Langmuir*, **26** [21] (2010) 16595–16606.
22. K. Murugappan, D.S. Silvester, D. Chaudhary, D.W. Arrigan, "Electrochemical characterization of an oleyl-coated magnetite nanoparticle-modified electrode", *Chem. Electro. Chem.*, **1** [7] (2014) 1211–1218.
23. J. Han, J. Meeprasert, P. Maitarad, S. Namuangruk, L. Shi D. Zhang, "Investigation of the facet-dependent catalytic performance of Fe_2O_3/CeO_2 for the selective catalytic reduction of NO with NH_3", *J. Phys. Chem. C.*, **120** [3] (2016) 1523–1533.
24. J.M. López, A.L. Gilbank, T. García, B. Solsona, S. Agouramand, L. Torrente-Murciano, "The prevalence of surface oxygen vacancies over the mobility of bulk oxygen in nanostructured ceria for the total toluene oxidation", *Appl. Catal. B: Environ.*, **174** (2015) 403–412.
25. A.G. Nasibulin, S. Rackauskas, H, Jiang, Y. Tian, P.R. Mudimela, S.D. Shandakov, L.I. Nasibulina, S. Jani, E.I. Kauppinen, "Simple and rapid synthesis of α-Fe_2O_3 nanowires under ambient conditions", *Nano Res.*, **2** [5] (2009) 373–379.
26. A.S. Reddy, C.Y. Chen, C.C. Chen, S.H. Chien, C.J. Lin, K.H. Lin, C.L. Chen, S.C. Chang, "Synthesis and characterization of Fe/CeO_2 catalysts: epoxidation of cyclohexene", *J. Mol. Catal. A: Chem.*, **318** [1] (2010) 60–67.
27. F. Zhang, P. Wang, J. Koberstein, S. Khalid, S.W. Chan, "Cerium oxidation state in ceria nanoparticles studied with X-ray photoelectron spectroscopy and absorption near edge spectroscopy", *Surface Sci.*, **563** [1] (2004) 74–82.
28. S. Babu, R. Thanneeru, T. Inerbaev, R. Day, A.E. Masunov, A. Schulte, S. Seal, "Dopant-mediated oxygen vacancy tuning in ceria nanoparticles", *Nanotechnology*, **20** [8] (2009) 085713.
29. A.P. Grosvenor, B.A. Kobe, N.S. McIntyre, "Examination of the oxidation of iron by oxygen using X-ray photoelectron spectroscopy and QUASES TM", *Surface Sci.*, **565** [2] (2004) 151–162.
30. M. Aronniemi, J. Sainio, J. Lahtinen, "Chemical state quantification of iron and chromium oxides using XPS: the effect of the background subtraction method", *Surface Sci.*, **578** [1] (2005) 108–123.
31. X. Wang, Z. Jiang, B. Zheng, Z. Xie, L. Zheng, "Synthesis and shape-dependent catalytic properties of CeO_2 nanocubes and truncated octahedral", *Cryst. Eng. Comm.*, **14** [22] (2012) 7579–7582.
32. X. Yao, C. Tang, Z. Ji, Y. Dai, Y. Cao, F. Gao, L. Dong, Y. Chen, "Investigation of the physicochemical properties and catalytic activities of $Ce_{0.67}M_{0.33}O_2$ (M = Zr^{4+}, Ti^{4+}, Sn^{4+}) solid solutions for NO removal by CO", *Catal. Sci. Technol.*, **2013** [3] (2013) 688–698.
33. Anushree, S. Kumar, C. Sharma, "$Ce_{1-x}Co_xO_y$ nanocatalysts: synthesis, characterization and environmental appli-

cation", *Catal. Sci. Technol.*, **6** [7] (2016) 2101–2111.
34. A. Heponiemi, L. Rahikka, U. Lassi, T. Kuokkanen, "Catalytic oxidation of industrial wastewater under mild conditions", *Topics Catal.*, **54** [16-18] (2011) 1034–1041.
35. A. Heponiemi, S. Azalim, T. Hu, U. Lassi, "Cerium oxide based catalysts for wet air oxidation of bisphenol A", *Topics Catal.*, **58** [14-17] (2015) 1043–1052.
36. S. Yang, W. Zhu, J. Wang, Z. Chen, "Catalytic wet air oxidation of phenol over CeO_2-TiO_2 catalyst in the batch reactor and the packed-bed reactor", *J. Hazardous Mater.*, **153** [3] (2008) 1248–1253.
37. M.S. Lucas, J.A. Peres, "Removal of COD from olive mill wastewter by Fenton's reagent: Kinetic study", *J. Hazardous Mater.*, **168** [2-3] (2009) 1253–1259.